

Article

# Radio Channel Scattering in a 28 GHz Small Cell at a Bus Stop: Characterization and Modelling

Manuel García Sánchez \* , Alejandro Santomé Valverde and Isabel Expósito 

Signal Theory and Communications Department, AtlanTTic Research Center, University of Vigo, 36310 Vigo, Spain; asantomevalverde@gmail.com (A.S.V.); iexpositop@uvigo.es (I.E.)

\* Correspondence: manuel.garciasanchez@uvigo.es

Received: 7 July 2020; Accepted: 21 September 2020; Published: 23 September 2020



**Abstract:** The 28 GHz band is one of the available bands in Frequency Range 2 (FR2), above 6 GHz, for fifth generation (5G) communications. The propagation characteristics at this frequency band, together with the bandwidth requirements of 5G communications, make it suitable for ultra-dense smart cell networks. In this paper, we investigate the performance of a radio channel in the presence of moving, scattering sources for a small cell at 28 GHz, located at a bus stop. To do so, measurements of the channel complex impulse response with a sweep time delay cross-correlation sounder were made and then used to examine the distribution of multipath components. Besides analyzing the delay spread caused by the channel, we also evaluate the impact on the Doppler spectrum (DS) caused by the vehicles passing near the bus stop. We show that delay components are grouped in clusters exhibiting exponential decay power. We also show that the DS varies with time as vehicles pass by, so the channel cannot be considered stationary. We propose an empirical DS model, where the model parameter should change with time to describe the non-stationary nature of the radio channel. We have also found that the DS with maximum spread is similar for channel contributions in different delay clusters.

**Keywords:** 5G; millimeter waves; radio channel; scattering; measurements; non-stationary channel

## 1. Introduction

The fifth generation (5G) of mobile communication systems is expected to meet a set of requirements identified by the industry [1–3]:

- 1–10 Gbps connections to end-points in the field;
- 1 ms end-to-end round-trip delay (latency);
- 1000 times increase of bandwidth per unit area;
- 10–100 times increase in the number of connected devices;
- (Perception of) 99.999% availability;
- (Perception of) 100% coverage;
- 90% reduction in network energy usage;
- Up to ten years of battery life for low power, machine-type devices.

The number of requirements to be fulfilled simultaneously will depend on each application and service. Enhanced mobile broadband (eMBB) services, for example, will take advantage of the high transmission bandwidths, although they may not require 1 ms latency times.

Due to the spectrum congestion below 6 GHz in Frequency Range 1 (FR1), the high bandwidths required for high-speed connections can only be found in the microwave and millimeter wave (mmWave) frequency bands of Frequency Range 2 (FR2) [4]. Among these candidate bands, the 28 GHz frequency

band is the one considered in our study. In this frequency region, the high free-space propagation losses, together with the high noise levels associated with large bandwidths, would yield low signal-to-noise ratios, unless directional antennas are used.

The use of directional steerable antennas at both channel ends has been proposed [5–9] for 5G systems at mmWave frequencies. This represents an important change in mobile communication systems, where omnidirectional antennas have traditionally been used, at least at mobile terminals. As the radio channel characteristics depend on the antenna pattern [10], new measurements are required to properly determine the channel characteristics for directional antennas. However, smart antennas are complex and still expensive in terms of cost and energy consumption. Thus, despite the original premises of 5G mobile communication systems, current 5G rollouts are centered on FR1, while FR2 will eventually support fixed access [11].

In addition to high mmWave attenuation, the requirement to increase the available bandwidth per unit area has raised the need for ultra-dense small cell networks [12]. These are low-powered radio access points with coverage areas of around a 100 m radius and an inter-site distance of 200 m. This allows frequency reuse on an extremely dense basis. Small cells will be a crucial component of 5G networks because they increase network capacity, density and coverage [13]. The 28 GHz band has been proposed for these small cells [12].

Radio channel characterization and modeling are of the utmost importance for wireless communications, as communication systems have to be designed to reach the desired performance levels under the impairments introduced by the radio channel. Power delay profiles (PDP) and the Doppler spectrum (DS) are important parameters to estimate both time and frequency dispersion introduced by a radio channel. Delay dispersion, if not mitigated adequately, may give rise to inter-symbol interference that may limit the capacity of the channel, while the DS is important for analyzing the time variance of the radio channel. Despite most studies considering a narrowband characterization of the DS, since the first works on wideband propagation [14], it has been well known that the DS may be different for different delay contributions.

The number of papers in the literature reporting fixed-to-fixed (F2F) outdoor radio channel measurements in the presence of moving scatterers is limited. For instance, in [15], the results of wideband measurements in a suburban environment at 2480 MHz are presented, but the Doppler analysis was not made separate for the different delayed components. More frequently, the DS is obtained from narrowband measurements, as in [16], where measurements in the presence of fast traffic on a motorway are reported, and in [17], where the moving scatterers are wind-blown leaves. At higher frequencies, like in [18], we find empirical results at 29.5 GHz.

The literature includes a series of wideband models for 5G radio channels that take delay dispersion into account. Such models can be classified [19] as deterministic, map-based (like METIS [20,21]) and stochastic. These can be further classified as geometry-based stochastic models, like COST2100 [22], WINNER+ [23] and 3GPP [24], or non-geometry-based stochastic models, such as the Saleh-Valenzuela model [25]. However, this is not a clear-cut division, as some models incorporate both deterministic and stochastic characteristics, like IEEE 802.11ay [26] and MiWEBA [27]. All of them are wideband models that provide an estimation of a channel's PDP.

Regarding the DS, we should mention specific geometrical-based stochastic models (GBSMs), which were developed for mobile communication channels and assume a particular geometrical distribution of static scatterers around the propagation environment. The classic Jakes model is one of these, but more sophisticated models include the one-ring [28], disk [29] and elliptical [30] models. In the one-ring model, scatterers are uniformly distributed on a thin ring, whereas for the disk model, they are distributed on a disk, being centered on the mobile station in both cases. For the elliptical model, scatterers are distributed on an ellipse, and the mobile and base stations are located on its foci. It should be noted that propagation paths suffering single scattering on the ellipse will have the same delay. Ring and disk models may be more adequate for narrowband systems, while the ellipse model would perform better for wideband ones [31].

The presence of moving scatterers was considered in [32], where a general vehicle-to-vehicle model was developed, considering random scatterer velocities with Gaussian and mixed Gaussian distributions. In this paper, it is assumed that waves can propagate from transmitter to receiver after a single bounce on the moving scatterer. The F2F channel model is obtained by particularizing the vehicle-to-vehicle model to the case in which the vehicle velocities are equal to zero. The application of the ring, disk and elliptical models to the case of an F2F radio channel can be found in [33]. The models are compared with measurement results at 29.5 GHz from [18] and measurement results at 5.8 GHz from [34].

Models for F2F links with a single moving scatterer can be found in [33], where a model is also proposed for the case of a non-uniform scattering pattern. The corresponding DS shows good agreement with measurement results performed with a wideband MIMO sounder in an indoor environment at 5.8 GHz.

In this paper, we consider the case of a small cell at 28 GHz deployed at a bus stop. We have measured the channel impulse response in this scenario using a wideband channel sounder. Despite using fixed antennas, the scenario cannot be considered static. The presence of moving scatterers, such as vehicles passing by the bus stop, could have a significant impact on channel behavior [35]. Particularly, moving objects will have an impact on the Doppler spread of the radio signals. It should be noted that this effect could be strong due to the linear dependency of the Doppler shift on the carrier frequency [36]. We analyze both the delay and the Doppler spread produced by the radio channel. Moreover, as the channel may have non-stationary behavior, we analyze the Doppler spectrum variation as vehicles pass by the bus stop.

There are several novel aspects in the paper. First, we provide wideband results for an F2F outdoor environment at 28 GHz, including the PDP and DS. Second, we obtain the DS separately for the main delay contributions. Third, we analyze the temporal variation of the DS, showing that the channel exhibits non-stationary behavior. Finally, we determine the requirements a model of this radio channel should comply with.

After this introductory section, the rest of the paper is organized as follows. In Section 2, we describe the measurement system and measurement environment. In Section 3, we present the measurement results. Finally, in Section 4, we summarize the conclusions of this work.

## 2. Experimental Set-Up

### 2.1. Channel Sounder

The experimental set-up was based on a sweep time delay cross-correlation channel sounder. This sounder consisted of a signal transmitter and a receiver. At the transmitter, we first generated a pseudorandom binary sequence of  $2^{12} - 1$  bits at a 900 Mbps rate, using an 81180A arbitrary waveform generator from Agilent. Figure 1 shows a capture of its spectrum. Then, we used this sequence to phase modulate a carrier at 28.65 GHz as follows. The output of the arbitrary generator was introduced as an input of an SMR40 microwave signal generator from Rohde & Schwarz, obtaining a modulated radio frequency (RF) signal with the spectrum in Figure 2. An ERZ-HPA-2700-4200-27 power amplifier from Erzia was used to reach a signal with a +27 dBm level, and it was finally transmitted with a directional pyramidal horn antenna with a gain of 20 dBi. This results in a high transmitted power for a small cell, but provides a good dynamic range to be able to analyze in detail small power contributions.

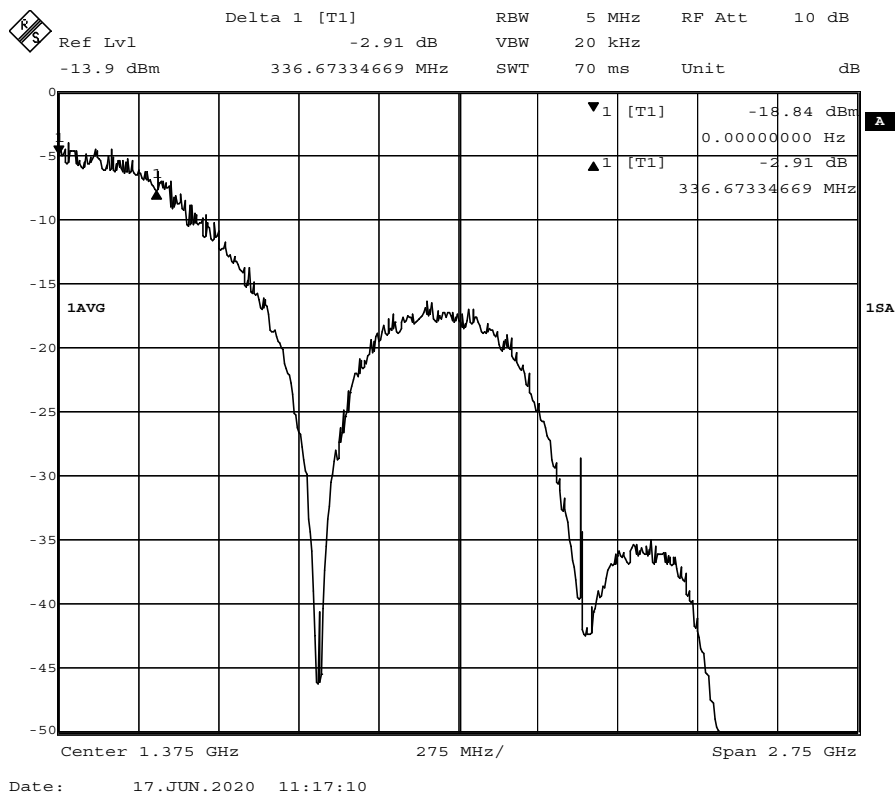


Figure 1. Measured baseband spectrum of the pseudorandom binary sequence.

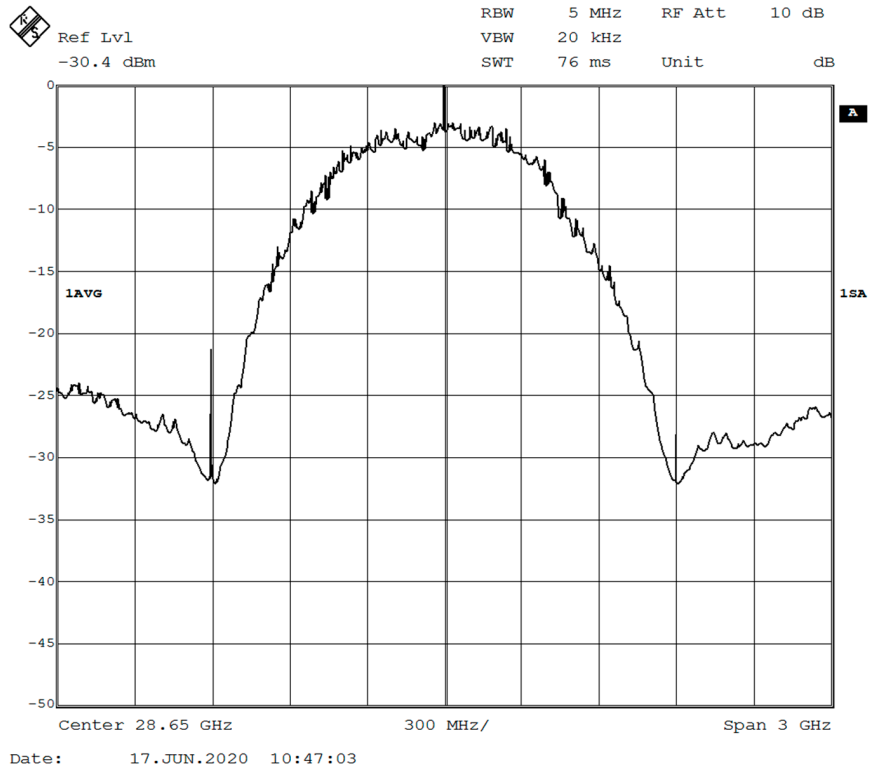


Figure 2. Measured spectrum of the modulated signal.

We used an omnidirectional antenna at the receiver to capture the RF signal. The signal passed first through an AMF-3F-26004000-25-13P low-noise amplifier from Miteq, and thereafter it was mixed

in a Miteq M1826W1 double-balanced mixer with a 28.15 GHz signal from a local oscillator to achieve an intermediate frequency (IF) of 500 MHz. The 28.15 GHz signal was generated from a 10 MHz signal we got from a PRS10 Rubidium clock from SRS Inc. that fed a DLCRO-10-14075, and then a MAX2M200400-20P frequency doubler, both from Miteq. Figure 3 shows a picture of the receiver, identifying each element. The IF signal was sampled at 5G samples/s using a digitizing oscilloscope, model DSO-S-104A from Keysight, and stored for further off-line processing. Each signal record lasted for 0.1058 s and therefore contained 529 M samples.

All signal generators and oscillators at the transmitter and the receiver were locked to the rubidium frequency standard. This was a very stable clock that guaranteed the measured delays could not be affected by any frequency variation of any oscillator, so they corresponded to actual wave propagation delays.

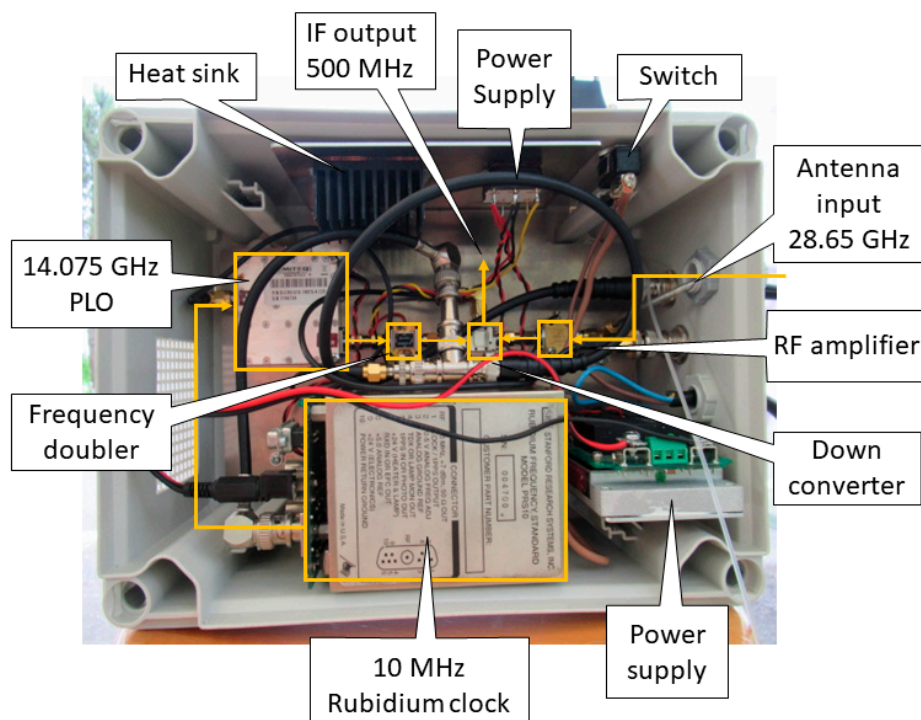


Figure 3. Receiver.

## 2.2. Measurement Scenario

Figure 4 shows a full picture of the set-up. We placed the directional transmitting antenna at a 2.5 m height beside the bus stop pole. The transmitting antenna was pointed toward the receiving one (see Figure 5), positioned on a stool inside the bus stop shelter, at a 0.9 m height. The horizontal distance between both antennas was 7 m. The most meaningful distances among the different elements in the measurement setup are included in Figure 6. Several signal records were obtained as different vehicles, including cars, vans and buses, passed by the bus stop, i.e., in the presence of scattering sources with different sizes and shapes (see Figure 4, Figure 7 and Figure 11).

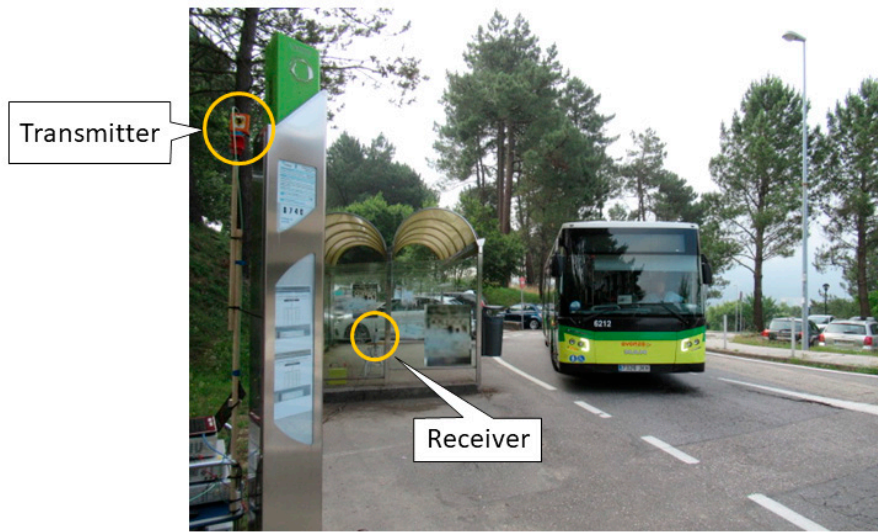


Figure 4. Transmitter and receiver at the bus stop.



Figure 5. Transmitting antenna by the bus stop pole.

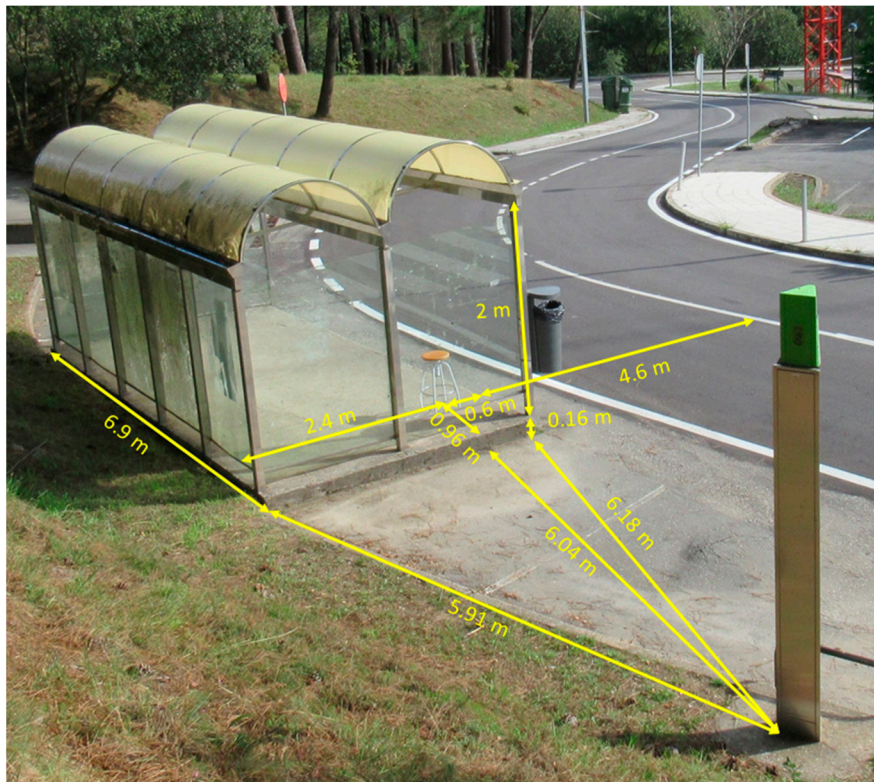


Figure 6. Environment dimensions.



Figure 7. A van passing by the bus stop.

### 2.3. Data Processing

Off-line processing was carried out to first demodulate the IF signal to baseband and then to perform the cross-correlation with an exact replica of the transmitted pseudo-random binary sequence. The result was the time-varying complex impulse response of the radio channel  $h(t,\tau)$  with a delay resolution of  $\Delta\tau = 1.11$  ns (1/900 MHz), which let us resolve a propagation path with a length difference of 0.33 m. The impulse response was obtained every  $\Delta t = (2^{12} - 1)/900$  MHz = 4.55  $\mu$ s, which corresponded to a sampling frequency of around 220 KHz. Increasing the sequence length would result in an improved dynamic range, but would reduce the sampling rate in the time domain. This fast sampling rate in the time domain allowed analysis of the temporal variations of some channel characteristic functions, such as the DS.

## 3. Results

### 3.1. Delay Spread

The most immediate result from the measurement processing, as explained in the previous section, was the time-varying complex impulse response of the radio channel. In Figure 8, we plot the normalized amplitude of this impulse response for the record, corresponding to the van passing by the bus stop (Figure 7). Contributions of up to 40 dB below the main one have been measured. In Figure 9, we present the corresponding PDP, resulting from averaging the squared amplitude of the impulse responses.

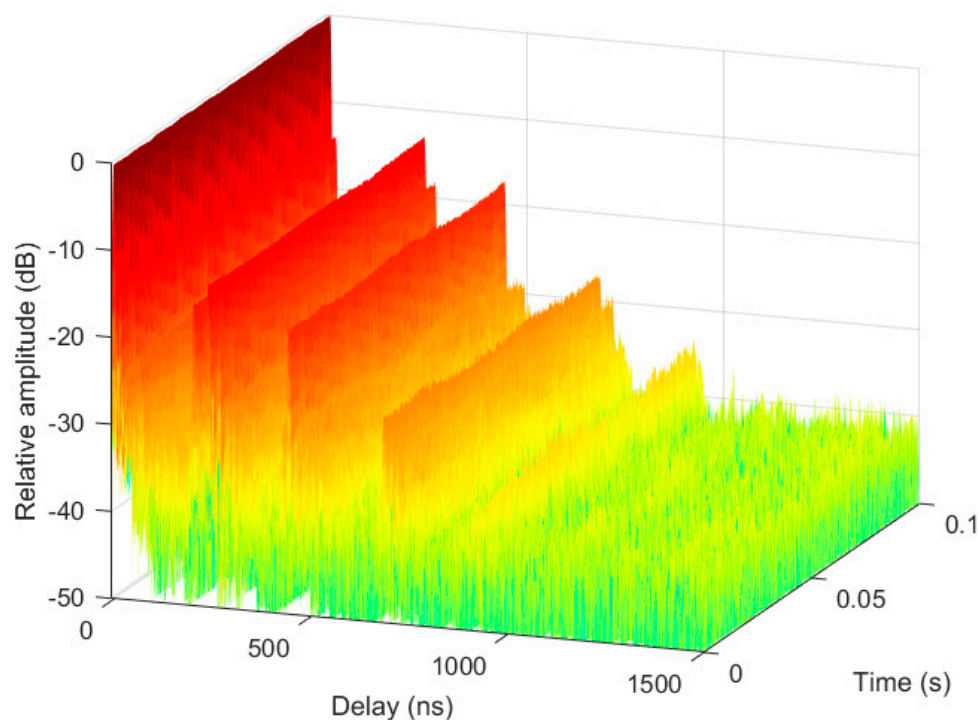
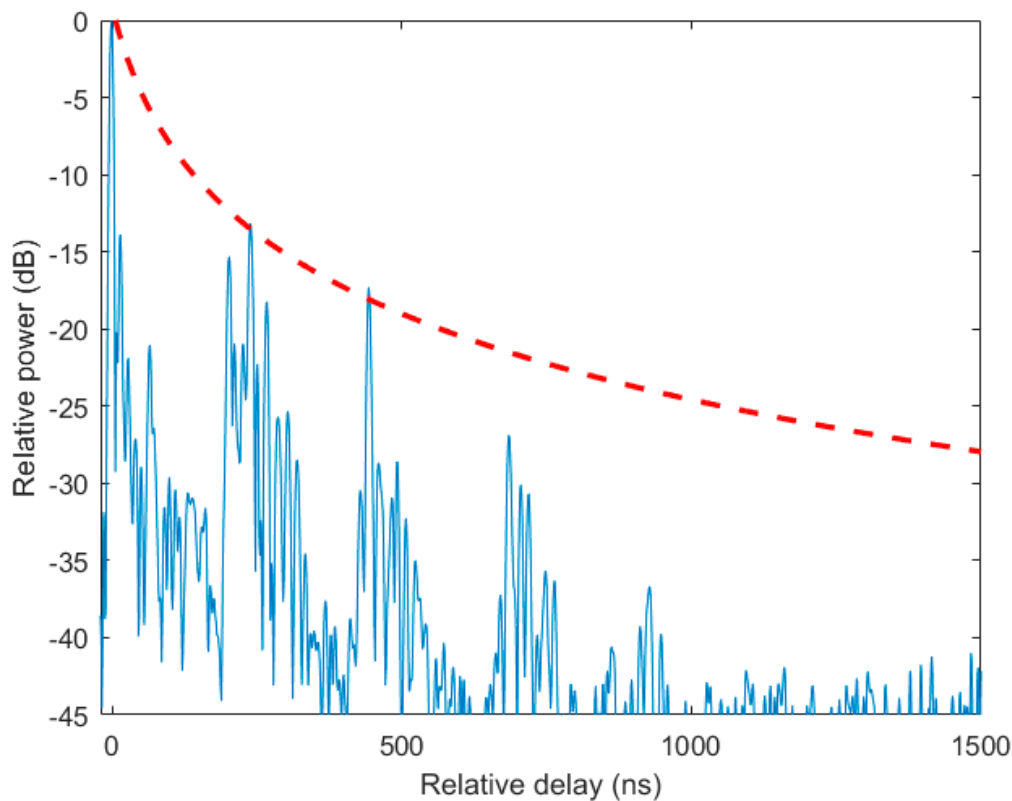


Figure 8. Amplitude of a measured time-varying impulse response.



**Figure 9.** Power delay profile (solid blue line) and free-space (red dashed line) power decay.

Several contributions with different delays and time-varying amplitudes grouped in clusters were appreciated. The different clusters were generated by propagation paths with very different lengths, while the components within a cluster were due to scattering objects surrounding the receiver or the transmitter. The power of the clusters varied with time. This may be not so clear for the zero-delay contribution, as there was a strong, direct component that dominated the propagation, but it could be seen for contributions with higher delays. This may suggest the channel is not stationary, as will become more evident after analyzing the DS.

According to the measurement geometry, the contributions from the direct path and the path with a single reflection on the vehicle are included in the first cluster. A cluster with larger delays should be due to contributions with multiple reflections on the vehicle and other fixed scatterers present in the environment.

The power of the clusters was reduced as the delay increased. The main contribution of each cluster decayed with the delay at a rate that was equal to or larger than the corresponding free-space losses for the equivalent distance. This is shown in Figure 9, where we have also plotted, in a thick, dashed red line, the free-space power decay with distance and delay.

Within each cluster, the power relative to the main contribution in the cluster also decreased with the excess delay, but at a larger rate than that corresponding to the free space. This behavior is widely described in the literature and has even been incorporated into different channel models, like the Saleh-Valenzuela model [25], the Winner+ model [23] and the ETSI-3GPP model [24].

However, we have found that a linear fit better approximates the power decay (in dB) of the main contribution in each cluster with distance, as seen in the upper graph of Figure 10. The regression line has a negative slope of  $-0.0379$ . Other captured records yield similar PDPs. For instance, the bottom graph in Figure 10 represents the PDP corresponding to the case of a car passing by the bus stop, as seen in Figure 11. Here, we can also identify the five clusters with decreasing power. The slope of the fitted line is  $-0.0343$ .

This agrees with the results presented in [37], where the empirical PDP obtained in urban environments at 1.8 GHz is modelled by a one-sided exponential decaying function:

$$PDP(\tau) \propto \begin{cases} \exp\left(-\frac{\tau}{\sigma_D}\right), & \text{for } \tau > 0 \\ 0, & \text{otherwise} \end{cases}, \quad (1)$$

This corresponds to a linear decay in logarithmic units.

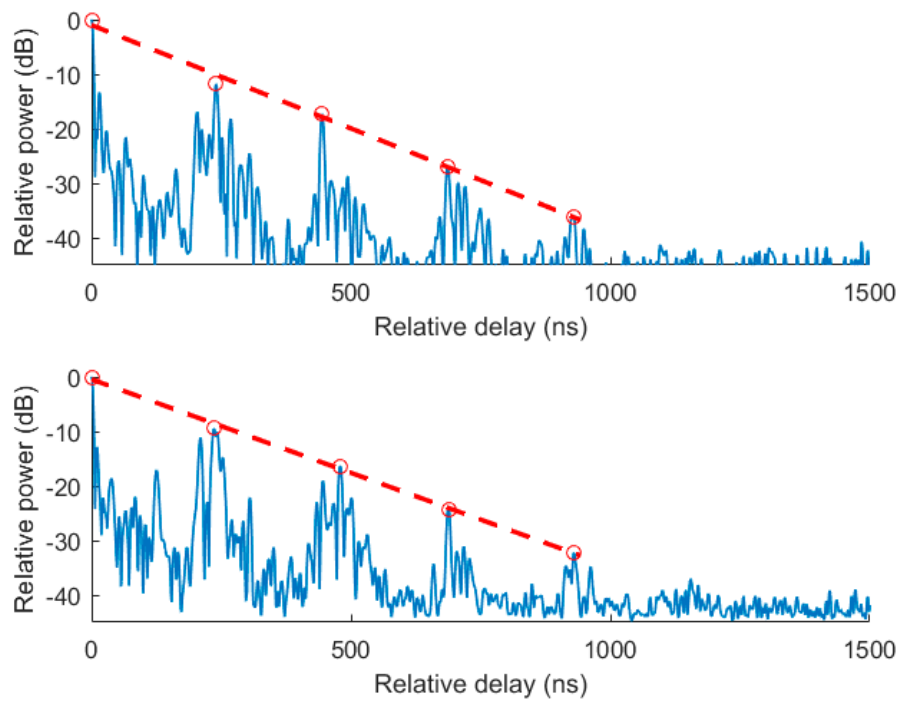


**Figure 10.** Power delay profile (solid blue line) and fitted (red dashed) line for the records of a van (upper graph) and a car (bottom graph).



**Figure 11.** Car passing by the bus stop.

### 3.2. Doppler Spectrum

To analyze the time-varying characteristics of the radio channel, we have calculated the Doppler spectrum corresponding to the time variation of the strongest components present in the complex impulse response. First, we identified the delay,  $\tau_i$ , of the main contributions in the PDPs. Then, we took each of the 0.1058 s time records of the time-varying impulse response corresponding to those delays with  $h(t, \tau_i)$ . We divided each record into 11 sections of 2048 samples, lasting 9.33 ms each, and calculated the correlation function, and the associated Doppler spectrum, for each section. In Figure 12, we plot the results for the eleven sections of the main component, the one with a relative delay of  $\tau_i = 0$  ns, coming from the same record of a car.

As can be seen, the DS shapes resemble those in the literature for F2F links in the presence of moving scatterers. However, the Doppler spectra change with time. When the car is far away from the sounder (solid thick blue line), the DS is quite narrow. This is clearly due to the filtering effect of the directive antenna pattern already described in [36,38]. However, as the car approaches the sounder, the Doppler spectrum is broadened, reaching a maximum broadening as shown in the dashed, thick red line. As there are significant DS changes with time, the channel cannot be considered stationary. This is reasonable because the incidence and observation angles change as the vehicle moves, and this will change the measured field scattered by the vehicle. A non-stationary model approximation would be needed. Any model would require a spread factor that varies with time as the vehicle moves.

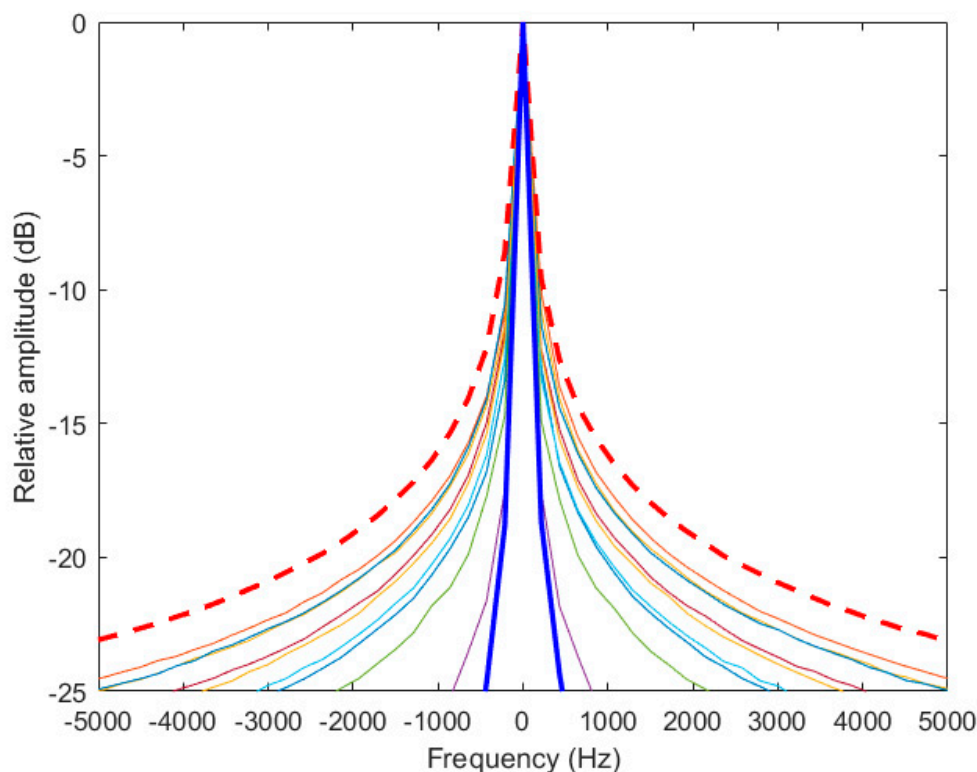


**Figure 12.** Time-varying Doppler spectrum for the main component ( $\tau_i = 0$  ns). Each drawn line corresponds to a different time interval.

In the literature, there are several DS models of F2F links in presence of moving scatterers. Closed-form expressions are given in [32] for an environment where the transmitter and receiver are in a fixed position and surrounded by a large number of moving scatterers. The emitted wave is supposed

to reach the receiver after a single bounce on the moving scatterer. Isotropic scattering is also assumed. Under these hypotheses, it is shown that for a constant velocity,  $v$ , of the scatterers, the DS will be

$$DS(f) = \frac{\sigma^2}{\pi^2 f_d} K \left( \sqrt{1 - \left( \frac{f}{2 f_d} \right)^2} \right) \quad (2)$$

where  $\sigma^2$  is the average received power,  $f_d$  is the maximum Doppler frequency, being  $f_d = v/\lambda$ ,  $\lambda$  is the wavelength and  $K$  denotes the complete elliptic integral of the first kind. However, if  $v$  is a random variable with exponential distribution and mean value  $v_m$ , then

$$DS(f) = \frac{\sigma^2}{\pi^2 f_m} K_0 \left( \frac{|f|}{2 f_m} \right) \quad (3)$$

where  $f_m = v_m/\lambda$  and  $K_0$  represents the zeroth-order modified Bessel function of the second kind.

The case of an F2F link with a single moving scatterer is presented in [34]. If the scatterer has a constant scattering cross-section and is moving in one direction, then

$$DS(f) = \frac{2}{\sqrt{1 - \left( \cos(\beta) + \frac{f}{f_d} \right)^2}} \quad (4)$$

where  $\beta$  is related to the direction of movement. If, however, it is moving in many directions, then

$$DS(f) = \frac{1}{\pi^2} K \left( \sqrt{1 - \left( \frac{f}{2 f_d} \right)^2} \right) \quad (5)$$

which differs from (2) in just an amplitude scaling factor. Finally, for non-uniform scattering patterns, an empirical model is proposed which, according to [33], will result in

$$DS(f) = \frac{1}{1 + s f^2} \quad (6)$$

where  $s = 1/(\sqrt{2} f_m)$ .

Despite all these models resulting in a peaky DS, none of them fit our measurements. This is not surprising, as our case of study does not comply with all the hypotheses under which these closed forms were obtained. However, we have defined an empirical DS model of the form

$$DS(f) = \frac{1}{\sqrt{1 + s f^2}} \quad (7)$$

which fits the measured results if the appropriate  $v_m$  is chosen. For instance, (7) fits the DS in the red dashed line in Figure 12 for  $v_m = 15$  km/h. This is shown in Figure 13, where we again plotted the red dashed line from Figure 12 and the one obtained from (7) in black dots. The model given by (7) can be fitted to the other curves in Figure 12 just by reducing the Doppler spread, i.e., by reducing  $v_m$ .

The time variation of the DS is also present in components corresponding to larger delays, showing a similar time-varying behavior as the main component. In Figure 13, we have plotted the Doppler spectra with maximum frequency spreads for the three main delay contributions of the same car measurements. As can be seen, the DSs with the maximum spread for each delay are very similar. This is not strange, as the DS is produced by wave scattering when the transmitted signal impinges on the moving vehicle. Further scattering on fixed objects, which gives rise to delayed clusters, should not modify the signal Doppler spread.

A complete scattering model for this channel should account for clustering of the contributions with different delays, as well as the Doppler spread for each delay component. The Doppler spread model for each component could be the same and even have the same parameter values, but should account for the non-stationary nature of the channel by varying the  $v_m$  value in (7).

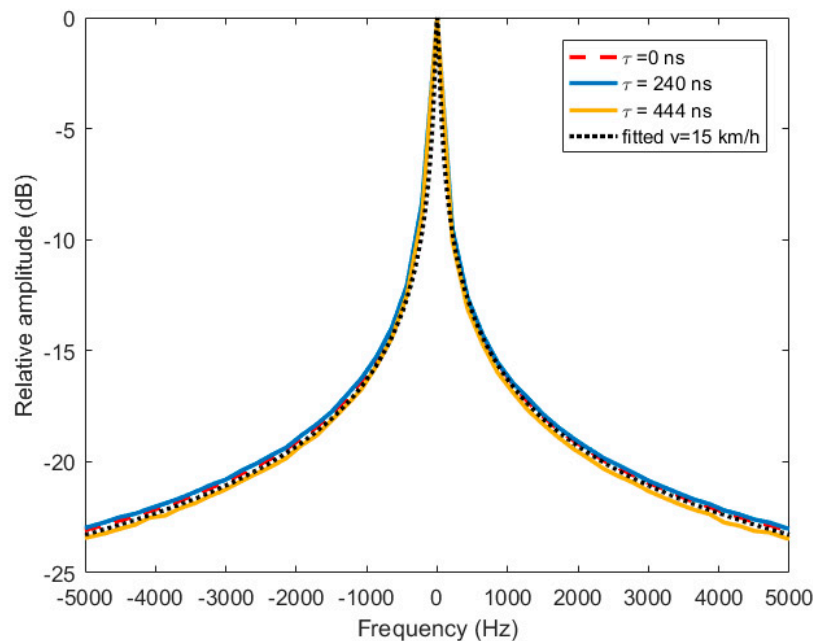


**Figure 13.** Doppler spectrum for the maximum frequency spread reached in components with relative delays  $\tau_i = 0$  ns,  $\tau_i = 240$  ns and  $\tau_i = 444$  ns, and the fitted model from (7).

#### 4. Conclusions

We have built and used a wideband radio channel sounder to characterize the radio channel for a small cell at 28 GHz. This is a very fast sounder, capable of performing the measurement of the channel impulse response every 4.55  $\mu$ s.

The small cell was deployed at a bus stop, and the impulse response was measured as different vehicles passed by. We have characterized the radio channel by determining its characteristic functions. We have shown that the multipath contributions group into clusters that present decreasing power with the delay. The power decay from the main components in the clusters follows a linear trend. Looking at the contributions within each cluster, decreasing power with the delay is also found.

Despite the DS being confined by the directional antenna used at the transmitter, we have shown that its spectrum varies with time as vehicles pass by the bus stop, reaching Doppler shifts that range from almost 0 Hz to a few kHz. The channel cannot be considered stationary, as the vehicle passed the bus stop. We conclude that a non-stationary DS model is needed, and that it should account for the Doppler spread variation with time by using a time-dependent spread factor value.

We have shown the requirements that a complete scattering model, accounting for both the delay and Doppler spreads, should meet for this radio channel. The delay spread should reflect the contribution clustering. The Doppler spread model for each delayed component could be the same and even have the same parameter values, but should account for the non-stationary nature of the channel. We propose an empirical model for the DS, where the non-stationary behavior of the channel can be reflected by varying the model parameter over time.

**Author Contributions:** Conceptualization, M.G.S.; methodology, M.G.S.; software, A.S.V.; formal analysis, M.G.S.; investigation, M.G.S., A.S.V. and I.E.; resources, I.E.; data curation, M.G.S.; writing—original draft preparation, M.G.S. and I.E.; supervision, M.G.S.; project administration, M.G.S.; funding acquisition, M.G.S. All authors have read and agreed to the published version of the manuscript.

**Funding:** This research was funded by the Spanish Government, Ministerio de Economía y Competitividad, Secretaría de Estado de Investigación, Desarrollo e Innovación, grant number TEC 2017-85529-C3-3-R; Xunta de Galicia, project ED431C 2019/26; atlantTTic Research Center and the European Regional Development Fund (ERDF).

**Conflicts of Interest:** The authors declare no conflict of interest. The funders had no role in the design of the study; in the collection, analyses, or interpretation of data; in the writing of the manuscript, or in the decision to publish the results.

## References

1. GSMA Intelligence. *Understanding 5G: Perspectives on Future Technological Advancements in Mobile*; GSMA Intelligence: London, UK, 2014.
2. Andrews, J.G.; Buzzi, S.; Choi, W.; Hanly, S.V.; Lozano, A.; Soong, A.C.; Zhang, J.C. What will 5G be? *IEEE J. Sel. Areas Commun.* **2014**, *32*, 1065–1082. [[CrossRef](#)]
3. Sánchez, M.G.; Portela, M.; Lemos, E. Millimeter wave radio channel characterization for 5G vehicle-to-vehicle communications. *Measurement* **2017**, *95*, 223–229. [[CrossRef](#)]
4. International Wireless Industry Consortium. *Evolutionary & Disruptive Visions towards Ultra High Capacity Networks White Paper*; International Wireless Industry Consortium: Doylestown, PA, USA, 2014.
5. Valliappan, N.; Lozano, A.; Heath, R.W. Antenna Subset Modulation for Secure Millimeter-Wave Wireless Communication. *IEEE Trans. Commun.* **2013**, *61*, 3231–3245. [[CrossRef](#)]
6. *IEEE Std 802.11ad-2012: Part 11: Wireless LAN Medium Access Control (MAC) and Physical Layer (PHY) Specifications: Amendment 3: Enhancements for Very High Throughput in the 60 GHz Band*; IEEE Computer Society: Washington, DC, USA, 2012.
7. El Ayach, O.; Heath, R.W.; Abu-Surra, S.; Rajagopal, S.; Pi, Z. The capacity optimality of beam steering in large millimeter wave. In Proceedings of the IEEE 13th International Workshop on Signal Processing Advances in Wireless Communications (SPAWC), Cesme, Turkey, 17–20 June 2012; pp. 100–104.
8. Kumari, P.; Gonzalez-Prelcic, N.; Heath, R.W. Investigating the IEEE 802.11ad Standard for Millimeter Wave Automotive Radar. In Proceedings of the IEEE 82nd Vehicular Technology Conference (VTC Fall), Boston, MA, USA, 6–9 September 2015.
9. Murad, N.A.; Raja Suleiman, R.F. Design of a ridged waveguide slot antenna for millimeterwave applications. In Proceedings of the IEEE International RF and Microwave Conference (RFM), Seremban, Negeri Sembilan, 12–14 December 2011; pp. 205–208.
10. Steele, R. *Mobile Radio Communications*; Wiley-Blackwell: Hoboken, NJ, USA, 1992.
11. Saad, W.; Bennis, M.; Chehri, M. A vision of 5G wireless systems: Applications, trends, technologies, and open research problems. *IEEE Netw.* **2020**, *34*, 134–142. [[CrossRef](#)]
12. Busari, S.A.; Mumtaz, S.; Al-Rubaye, A.; Rodríguez, J. 5G millimeter-wave mobile broadband: Performance and challenges. *IEEE Commun. Mag.* **2018**, *56*, 137–143. [[CrossRef](#)]
13. Small Cells Forum. Available online: [www.smallcellforum.org](http://www.smallcellforum.org) (accessed on 22 September 2020).
14. Cox, D. Delay Doppler characteristics of multipath propagation at 910 MHz in a suburban mobile radio environment. *IEEE Trans. Antennas Propag.* **1972**, *20*, 625–635. [[CrossRef](#)]
15. Baum, D.S.; Gore, D.; Nabar, R.; Panchanathan, S.; Hari, K.V.S.; Erceg, V.; Paulraj, A.J. Measurement and characterization of broadband MIMO fixed wireless channels at 2.5 GHz. In Proceedings of the 2000 IEEE International Conference on Personal Wireless Communications, Hyderabad, India, 17–20 December 2000; pp. 203–206.
16. Torres, R.P.; Cobo, B.; Mavares, D.; Medina, D.; Loredó, S.; Engels, M. Measurement and statistical analysis of the temporal variations of a fixed wireless link at 3.5 GHz. *Wirel. Pers. Commun.* **2006**, *37*, 41–59. [[CrossRef](#)]
17. Domazetovic, A.; Greenstein, L.J.; Mandayam, N.B.; Seskar, I. Estimating the Doppler spectrum of a short-range fixed wireless channel. *IEEE Commun. Lett.* **2003**, *7*, 227–229. [[CrossRef](#)]
18. Naz, N.; Falconer, D.D. Temporal variations characterization for fixed wireless at 29.5 GHz. In Proceedings of the 2000 IEEE 51st Vehicular Technology Conference Proceedings, Tokyo, Japan, 15–18 May 2000; pp. 2178–2182.
19. Sánchez, M.G.; Lemos, E.; Alejos, A.V. Empirical modeling of radiowave angular power distributions in different propagation environments at 60 GHz for 5G. *Electronics* **2018**, *7*, 365. [[CrossRef](#)]

20. METIS. METIS Channel Models. ICT-317669 METIS Project. 2015. Available online: [https://metis2020.com/documents/deliverables/METIS\\_D1.4\\_v1.0.pdf](https://metis2020.com/documents/deliverables/METIS_D1.4_v1.0.pdf) (accessed on 31 August 2020).
21. Medbo, J.; Kyosti, P.; Kusume, K.; Raschkowski, L.; Haneda, K.; Jamsa, T.; Nurmela, V.; Roivainen, A.; Meinila, J. Radio propagation modeling for 5G mobile and wireless communications. *IEEE Commun. Mag.* **2016**, *54*, 144–151. [[CrossRef](#)]
22. Liu, L.; Oestges, C.; Poutanen, J.; Haneda, K.; Vainikainen, P.; Quitin, F.; Tufvesson, F.; de Doncker, P. The COST 2100 MIMO channel model. *IEEE Wirel. Commun. Mag.* **2012**, *19*, 92–99. [[CrossRef](#)]
23. Meinila, J.; Kyosti, P.; Hentila, L.; Jamsa, T.; Suikkanen, E.; Kunnari, E.; Narandzic, M. D5.3: WINNER+ Final Channel Models. *Wirel. World Initiat. New Radio* **2010**, 119–172. Available online: <https://docplayer.net/34577643-D5-3-winner-final-channel-models.html> (accessed on 22 September 2020).
24. ETSI TR 138 900 V14.3.1 Study on Channel Model for Frequency Spectrum above 6 GHz (3GPP TR 38.900 Version 14.3.1 Release 14). Available online: <https://cdn.standards.iteh.ai/samples/53521/f79aa5eea08c43c1b6cc18f62baa26af/ETSI-TR-138-900-V14-3-1-2017-08-.pdf> (accessed on 22 September 2020).
25. Saleh, A.A.M.; Valenzuela, R. A statistical model for indoor multipath propagation. *IEEE J. Sel. Areas Commun.* **1987**, *5*, 128–137. [[CrossRef](#)]
26. Channel Models for IEEE 802.11ay, doc IEEE 802.11-15/1150r9. May 2016. Retrieved on 1st September 2020. Available online: [https://www.ieee802.org/11/Reports/tgay\\_update.htm](https://www.ieee802.org/11/Reports/tgay_update.htm) (accessed on 22 September 2020).
27. Weiler, R.J.; Peter, M.; Keusgen, W.; Maltsev, A.; Karls, I.; Puduev, A.; Bolotin, I.; Siaud, I.; Ulmer-Moll, A.M. Quasi-deterministic millimeter-wave channel models in MiWEBA. *EURASIP J. Wirel. Commun. Netw.* **2016**, *2016*, 84–99. [[CrossRef](#)]
28. Shiu, D.-S.; Foschini, G.J.; Gans, M.J.; Kahn, J.M. Fading correlation and its effect on the capacity of multielement antenna systems. *IEEE Trans. Commun.* **2000**, *48*, 502–513. [[CrossRef](#)]
29. Borhani, A.; Pätzold, M. A unified disk scattering model and its angle-of-departure and time-of-arrival statistics. *IEEE Trans. Veh. Technol.* **2013**, *62*, 473–485. [[CrossRef](#)]
30. Liberti, J.C.; Rappaport, T.S. A geometrically based model for line-of-sight multipath radio channels. In Proceedings of the Vehicular Technology Conference-VTC, Atlanta, GA, USA, 28 April–1 May 1996; pp. 844–848.
31. Patzold, M.; Hogstad, B.O. A wideband MIMO channel model derived from the geometric elliptical scattering model. In Proceedings of the 3rd International Symposium on Wireless Communication Systems (ISWCS), Valencia, Spain, 5–8 September 2006; pp. 138–143.
32. Borhani, A.; Pätzold, M. Correlation and spectral properties of vehicle-to-vehicle channels in the presence of moving scatterers. *IEEE Trans. Veh. Technol.* **2013**, *62*, 4228–4239. [[CrossRef](#)]
33. Zhao, X.; Han, Q.; Li, B.; Dou, J.; Hong, W. Doppler spectra for F2F radio channels with moving scatterers. *IEEE Trans. Antennas Propagat.* **2016**, *64*, 4107–4112. [[CrossRef](#)]
34. Andersen, J.B.; Nielsen, J.O.; Pedersen, J.O.; Bauch, G.; Dietl, G. Doppler spectrum from moving scatterers in a random environment. *IEEE Trans. Wirel. Commun.* **2009**, *8*, 3270–3277. [[CrossRef](#)]
35. Bian, J.; Sun, J.; Wang, C.X.; Feng, R.; Huang, J.; Yang, Y.; Zhang, M. A Winner+ based 3D non-stationary wideband MIMO channel model. *IEEE Trans. Wirel. Commun.* **2018**, *17*, 1755–1767. [[CrossRef](#)]
36. Lorca, J.; Hunukumbure, M.; Wang, Y. On overcoming the impact of Doppler spectrum in millimeter-wave V2I communications. In Proceedings of the IEEE Globecom Workshops, Singapore, 4–8 December 2017.
37. Pedersen, K.I.; Mogensen, P.E.; Fleury, B.H. A stochastic model of the temporal and azimuthal dispersion seen at the base station in outdoor propagation environments. *IEEE Trans. Veh. Technol.* **2000**, *49*, 437–447. [[CrossRef](#)]
38. Sanchez, M.G.; De Haro, L.; Pino, A.G.; Calvo, M. Human operator effect on wide band radio channel characteristics. *IEEE Trans. Antennas Propag.* **1997**, *45*, 1318–1320. [[CrossRef](#)]

